Broadband absorption spectroscopy in turbid media by combined frequency-domain and steady-state methods

Frédéric Bevilacqua, Andrew J. Berger, Albert E. Cerussi, Dorota Jakubowski, and Bruce J. Tromberg

A technique for measuring broadband near-infrared absorption spectra of turbid media that uses a combination of frequency-domain (FD) and steady-state (SS) reflectance methods is presented. Most of the wavelength coverage is provided by a white-light SS measurement, whereas the FD data are acquired at a few selected wavelengths. Coefficients of absorption (μ_a) and reduced scattering (μ_s') derived from the FD data are used to calibrate the intensity of the SS measurements and to estimate μ_s' at all wavelengths in the spectral window of interest. After these steps are performed, one can determine μ_a by comparing the SS reflectance values with the predictions of diffusion theory, wavelength by wavelength. Absorption spectra of a turbid phantom and of human breast tissue *in vivo*, derived with the combined SSFD technique, agree well with expected reference values. All measurements can be performed at a single source–detector separation distance, reducing the variations in sampling volume that exist in multidistance methods. The technique uses relatively inexpensive light sources and detectors and is easily implemented on an existing multiwavelength FD system.

OCIS codes: 170.1470, 170.4090, 170.5280, 170.7050.

1. Introduction

Reflectance spectroscopy is a technique for characterizing turbid media that has become widely used in medical diagnostics. In many cases the quantification of chromophore concentrations is desired, and this requires the ability to separate the effects of absorption from those of scattering. Fundamentally, the coefficients of absorption μ_a and of reduced scattering μ_s' can be determined by a series of reflectance measurements performed in one of three domains, namely, time[1–3] (with a fast pulse of light), frequency[4–7] (with a sinusoidally modulated source of light), and steady state[8–15] (with a source of constant intensity but multiple detectors at different distances). Unsurprisingly, these three techniques have different merits and limitations. Spatially resolved steady-state techniques are relatively inexpensive and are more readily suited for the determination of μ_a and μ_s' over large, continuous ranges of wavelengths than are the other methods. However, the steady-state approach works best when measurements are performed with a combination of short (~1 transport mean free path) and long (many transport mean free paths) source–detector separations.[11] Ideally, the optical properties of the sample should not vary over the ranges of volumes probed by the various measurements. The larger the spread of distances probed, the more likely that heterogeneities, such as those found in biological tissue, will distort the data from the predictions of the model. One approach to limiting this effect, given that the shortest separations provide great stability for the calculation of μ_s', is to use relatively short (<10-mm) source–detector separations.[12,13] Inasmuch as the mean probing depth scales with the source–detector separation, with this approach such measurements are sensitive to superficial components (to depths of less than 5 mm for typical biological tissues).

Time- and frequency-domain techniques are well suited for deeper (>1 cm for biological tissue) inves-

When this research was performed, all authors were with the Beckman Laser Institute, University of California, Irvine, Irvine, California 92612. A. J. Berger is now with The Institute of Optics, University of Rochester, Rochester, New York 14627. B. J. Tromberg's e-mail address is tromberg@bli.uci.edu.

Received 26 April 2000; revised manuscript received 18 August 2000.

0003-6935/00/346498-10$15.00/0

tigations. Moreover, they can be performed with only one or a few source–detector separations, which makes them more robust for use in studying heterogeneous samples. Because such techniques require sources that can be pulsed or modulated rapidly, covering a large wavelength range requires a tunable laser or an extensive collection of laser diodes, both of which can be expensive, difficult to maintain, and slow to cover the entire spectrum. This is an important drawback, because, as discussed by Hull *et al.*,[14] the quantification of chromophore concentrations can be significantly affected by use of a limited number of wavelengths.

In this paper we suggest a way to use steady-state (SS) and frequency-domain (FD) reflectance measurements in tandem to obtain broad wavelength coverage with increased penetration depth. This method is especially promising for near-infrared spectroscopy of tissue, e.g., to characterize breast physiology. For such applications, the method proposed here permits rapid data acquisition, deep tissue probing, and robust resolution of the contributions from the four major near-infrared tissue absorbers: oxyhemoglobin, deoxyhemoglobin, water, and fat. The central innovations are using FD-derived μ_a and μ_s' values to convert the SS measurements into units of absolute reflectance and using the power-law wavelength dependence of μ_s' to obtain interpolated and extrapolated values at nonlaser wavelengths. FD measurements are made at a handful of diode laser wavelengths spanning the range of interest (650–1000 nm), whereas the SS measurements are made continuously across the entire range. Unlike for spatially resolved SS, however, here only a single, large source–detector separation is used, preferably the same one as for the FD measurements. The instrumentation is straightforward and particularly easy to add to an existing FD system.

After describing our method of combining the SS and FD methods (SSFD), we test the SSFD technique by using it to measure the absorption spectra of turbid samples. First, we analyze a liquid tissue phantom whose absorption spectrum is known (by direct spectrophotometry of the absorbing component before mixing) and with which the SSFD result can be compared. We also measure locations on the breasts of two human female volunteers, demonstrating that data can be gathered *in vivo* and analyzed to provide pertinent physiological parameters. Differences among the measured breast spectra can be interpreted in terms of different relative levels of water, fat, and hemoglobin present in the explored tissue volumes. In addition, estimates of absolute concentrations are comparable with those reported in other recent broadband *in vivo* studies. Finally, we discuss possible reasons for imperfect spectral fits and compare concentration predictions derived from SSFD analysis with those derived from FD data alone.

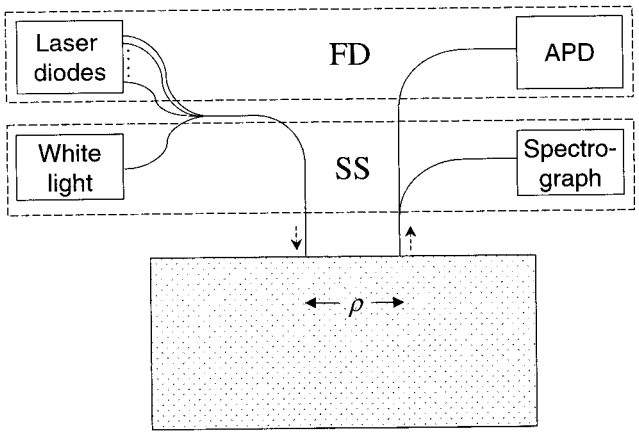

Fig. 1. Configuration of light sources, optical fibers, and detectors: APD, avalanche photodiode. The dashed rectangles denote components that belong to the FD and SS systems.

2. Experimental Methods

A. Optical Measurements

Figure 1 shows the experimental arrangement for SSFD measurements. In all cases, light is delivered via optical fiber to the surface of the sample and collected at some distance ρ away. For the liquid phantom measurements, ρ was 15.5 mm; for the breast, 21.5 (FD) and 24 (SS) mm (the slight difference was due to instrumental limitations; a future instrument will utilize identical distances). In FD mode (upper dashed rectangle), the light arrives sequentially from one of seven amplitude-modulated diode lasers (672, 800, 806, 852, 896, 913, and 978 nm, all with output powers of $<$20 mW at the sample) and is detected by an avalanche photodiode unit (Hamamatsu C556P-56045-03) that amplifies the ac component of the signal. A network analyzer (Hewlett-Packard 8753C) delivers 251 modulation frequencies from 100 to 700 MHz and measures phase and modulation amplitudes of the photon intensity signal, as described elsewhere.[7,16] In SS mode (lower dashed rectangle), light comes from a 150-W halogen lamp (Fiber-Lite) and is analyzed by a fiber-coupled spectrograph (Ocean Optics S2000) with a linear CCD detector from 525 to 1155 nm, with the useful range for our experiments being 650–1000 nm. The spectrograph records a total of 2048 points (0.35 nm/pixel), and the spectral resolution is 5 nm (full width at half-maximum). Light is delivered to the sample through a bundle of four fibers (bundle diameter, 600 μm) and collected with a single fiber of 1-mm diameter. We measure the spectrum of the light source separately by inserting the source and detector fibers into different ports of an integrating sphere (Labsphere, IS-040-SF). Relative reflectance is calculated to be the sample spectrum divided by the source spectrum (note that both measurements use the same delivery fiber, collection fiber, and detector apparatus). Total acquisition time per sample for SSFD measurements is of the order of 40 s (30 s for FD and 10 s for SS). We calculated $\mu_a(\lambda)$ according

to the methods of Section 3 with an in-house Matlab (The MathWorks, Inc.) code, making use of the optimization toolbox.

B. Samples

The phantom contained 17 mg of green dye (naphthol) and 50 mL of an aqueous scattering suspension (Intralipid-20%, Pharmacia, Inc.) dissolved in 950 mL of water. Before the addition of Intralipid, the absorbance spectrum of the dye–water solution was measured in a 1-cm plastic cuvette by a spectrophotometer (Beckman Instruments, DU630) with water as a reference. Optical measurements were performed as indicated in Fig. 1, with source and detector fibers placed at the surfaces of the samples.

In vivo measurements were performed on the left breasts of two supine female volunteers, aged 37 and 21 years. Data were gathered from two regions on one volunteer (a region on the areolar border and a region of inner breast, i.e., close to the middle of the chest) and from one region (inner breast only) on the other volunteer, yielding a total of three samples. In this modality, the source light was again delivered by optical fiber but the FD detector was placed directly against the tissue, without a collection fiber. Fiber and detector were bundled into a single hand-held device that was placed gently against the breast. SS reflectance was measured subsequently, at the exact same location, in the two-fiber mode described above. All procedures were approved by the Institutional Review Board of the University of California, Irvine (study 95-563).

3. Background Theory

A. Diffusion Model

The measured reflectance signal R can be predicted theoretically by use of the diffusion approximation to the radiative transfer equation, as many groups of researchers have discussed.[7,17–21] In this theoretical framework, the reflectance is a function of the optical properties of the medium, defined by absorption coefficient μ_a, reduced scattering coefficient μ_s', and index of refraction n. The diffusion approximation is valid for large source–detector separation r [$r > 10(\mu_a + \mu_s')^{-1}$] and high (reduced) albedo [$\mu_s'/(\mu_a + \mu_s') > 0.95$]. The SS and FD cases can be described by a single formalism in which the solution for the reflectance is built from the Green's function for the diffusion equation, i.e., the fluence [W/cm^2] that is due to an isotropic point source in an infinite, homogeneous medium. This function takes the form $\exp(-kr)/(Dr)$, where $D \equiv [3(\mu_a + \mu_s')]^{-1}$, the complex wave number is $k = k_{\text{real}} + ik_{\text{imag}}$, and

$$k_{\text{real}} = \left[\frac{3}{2}\,\mu_a(\mu_a + \mu_s')\right]^{1/2}\left\{\left[1 + \left(\frac{\omega}{\mu_a c}\right)^2\right]^{1/2} + 1\right\}^{1/2},$$

$$k_{\text{imag}} = \left[\frac{3}{2}\,\mu_a(\mu_a + \mu_s')\right]^{1/2}\left\{\left[1 + \left(\frac{\omega}{\mu_a c}\right)^2\right]^{1/2} - 1\right\}^{1/2},$$

where ω is the modulation frequency in radians per second. The steady-state solution is simply the limit when $\omega = 0$. In this case the solution for R is a real number $\{k_{\text{real}} = [3\mu_a(\mu_a + \mu_s')]^{1/2}$ and $k_{\text{imag}} = 0\}$. When $\omega > 0$, R becomes a complex number $A\exp(-i\phi)$, where A is the modulation amplitude and ϕ is the phase shift relative to the source. As we explain in Subsection 3.B, these quantities can be obtained from the FD measurement.

In treating reflectance problems, we model the sample–air interface, using an extrapolated boundary condition[21] in which the fluence is set to zero at a distance $z_b = 2D(1 + R_{\text{eff}})/(1 - R_{\text{eff}})$ above the sample (R_{eff} depends on the refractive mismatch and equals 0.493 for tissue of $n = 1.4$ and air of $n = 1.0$). The method of images is employed, with an isotropic point source at a depth $z_o = (\mu_a + \mu_s')^{-1}$ contributing a signal S_r and a negative image point at a height $z_o + z_b$ above the extrapolated boundary contributing S_i. The result is the fluence Φ at any point in the sample. The detected signal along the boundary is then written as a combination of terms proportional to the fluence and to its flux normal to the surface:

$$R = c_1\Phi - c_2 D\nabla\Phi\cdot(-\hat{z}), \tag{1}$$

where values for the constants c_1 and c_2 are determined by the refractive-index mismatch between the two media[21] (for tissue of $n = 1.40$ and air of $n = 1$, for these constants the values 0.118 and 0.306, respectively, are assumed), $-\hat{z}$ is a unit vector pointing normally upward out of the sample, and

$$\Phi = \frac{P}{4\pi D}\left[\frac{\exp(-kr_s)}{r_s} - \frac{\exp(-kr_i)}{r_i}\right],$$

$$D\nabla\Phi\cdot\hat{z} = \frac{P}{4\pi}\left[z_o\left(k + \frac{1}{r_s}\right)\frac{\exp(-kr_s)}{r_s^2} + (z_o + 2z_b)\times\left(k + \frac{1}{r_i}\right)\frac{\exp(-kr_i)}{r_i^2}\right], \tag{2}$$

where P is the incident power and r_s (r_i) is the distance from the source (image) to the detector.

B. Frequency-Domain Fitting

Like the theory of Subsection 3.A, our FD fitting process, which provides μ_a and μ_s' values at a few wavelengths, has been described at length elsewhere,[7,16] and a brief description is provided here as background.

Each FD measurement contains instrumental artifacts; i.e., the measured reflectance is actually

$$R = C_o A\exp[-i(\phi + \phi_o)], \tag{3}$$

where C_o and ϕ_o are sample-independent instrumental constants. A and ϕ are, respectively, the modulation amplitude and phase of the FD reflectance, as defined in Subsection 3.A.

For calibration, we gather FD data from a prepared sample whose μ_a and μ_s' values are known *a priori* from a set of two-distance FD measurements.[7]

Frequency-dependent values of ϕ_o and C_o are calculated from the discrepancies between measured [Eq. (3)] and predicted [Eq. (1)] phase and modulation amplitude, thus calibrating our future measurements.

With the instrumental constants thus determined, the 502 data points per sample (251 for both phase and amplitude as a function of the FD modulation frequency ω) depend on two unknowns, μ_a and μ_s'. We select the best μ_a and μ_s' values to fit the predictions of Eq. (1) to the data, using the iterative, nonlinear, least-squares method of Levenberg and Marquardt,[22] simultaneously fitting the phase and the amplitude until overall convergence is achieved.[7] As was noted by various authors,[2,21] the reflectance in Eq. (1) is nearly proportional to either the flux or the fluence term alone (i.e., the ratio of the two is independent of μ_a and μ_s') for the large source–detector separations that we employ [$>10(\mu_a + \mu_s')^{-1}$]. We therefore use only the fluence term Φ from Eq. (1), absorbing the additional proportionality factor into the instrumental constant C_o.

4. Determination of Broadband μ_a Spectrum

Section 3 provided background information regarding diffusion theory models and a method for extracting μ_a and μ_s' values from FD measurements at specific wavelengths. We now describe how FD and SS measurements can be combined to yield quantitative, broadband μ_a spectra.

Our goal is to compute μ_a at each wavelength, given the measured SS reflectance. However, single-distance SS reflectance cannot itself provide μ_a: R depends on μ_s' as well as on μ_a, so one measurement cannot provide a unique determination of either parameter. In addition, the instrumental constant C_o is not known. The single SS measurement at each wavelength therefore needs to be supplemented with both a means of establishing the absolute reflectance intensity and an additional piece of information about μ_a or μ_s' (or a combination of the two).

A. Use of Frequency-Domain Data to Provide Additional Information

The FD system can provide both pieces of necessary information at each SS wavelength. At first glance this is surprising, as the FD system operates at only seven wavelengths, whereas the SS system covers 450 nm with continuous 5-nm resolution. It would seem then that the needed values of μ_s' and C_o could be determined only at these seven wavelengths, and strictly speaking such is indeed the case. Significantly, however, the wavelength dependence of both μ_s' and C_o is smooth and predictable in shape, as is discussed below. It is this fact that enables us to use the discrete FD information to supplement our broadband SS measurements at all desired wavelengths.

B. Amplitude Calibration of the Reflectance Spectrum

The FD measurements permit calculation of the instrumental factor C_o at all wavelengths because we expect no wavelength dependence at all: The sample and source spectra are measured with the same delivery and collection system and only a few seconds apart, so there should be negligible wavelength-dependent artifacts in the ratio of the two. Therefore the task reduces to that of calculating C_o at a single wavelength. This is readily done at any of the FD wavelengths, as μ_a and μ_s' are both known and absolute reflectance is a function only of these variables [cf. Eqs. (1) and (2) in the $\omega = 0$ limit]. Using all the FD data to increase robustness, we can calculate the value of C_o that scales the measured SS reflectances to match the predicted reflectances as closely as possible (in the least-squares sense). Once this is done, the scale factor C_o is known for the entire spectrum. Examples of this scaling are given below.

C. Determination of $\mu_s'(\lambda)$

The FD values of μ_s' also allow us to obtain information about μ_s' across the entire wavelength range. As numerous groups of researchers have observed,[23–25] the particle size distribution of scatterers (0.1–10 μm) in many biological media and phantoms tends to have smooth wavelength dependence over the range 650–1000 nm, which is well described by a power function of the form

$$\mu_s'(\lambda) = A\lambda^{-B} \tag{4}$$

(the parameter A here has no relation to the modulation amplitude). As a result, measuring several μ_s' values allows us to fit those values to a simple function of wavelength and to obtain good estimates of μ_s' at all other wavelengths needed.

D. Iterative Solving for the $\mu_a(\lambda)$ Spectrum

With $\mu_s'(\lambda)$ calculated and the reflectance correctly scaled, the equation for steady-state reflectance ([Eq. (1)] contains only one unknown, μ_a. Because it is difficult to obtain an analytical solution for μ_a from this equation, numerical solving methods were employed. Proceeding one wavelength at a time, we used the Matlab nonlinear zero-finding function fzero to choose μ_a such that $R_{\mathrm{meas}} - R_{\mathrm{thy}}(\mu_a) = 0$, where R_{meas} is the calibrated SS reflectance measurement and $R_{\mathrm{thy}}(\mu_a)$ is the theoretical reflectance predicted by Eqs. (1) and (2) for a given trial value of μ_a. Solving for the entire μ_a spectrum required $\sim$10 s on a personal computer.

5. Results

Figure 2 displays the SS reflectance measured from the phantom and the predicted absolute reflectance calculated from diffusion theory based on the FD measurements of μ_a and μ_s'. Because of strong absorption at wavelengths above 950 nm, the FD measurement at 978 nm was noisy, which in turn made the calculation of SS data at wavelengths above 950 unstable. Data are therefore presented for 650–950 nm for the phantom only. As anticipated, all the measurements differ from the predictions by essen-

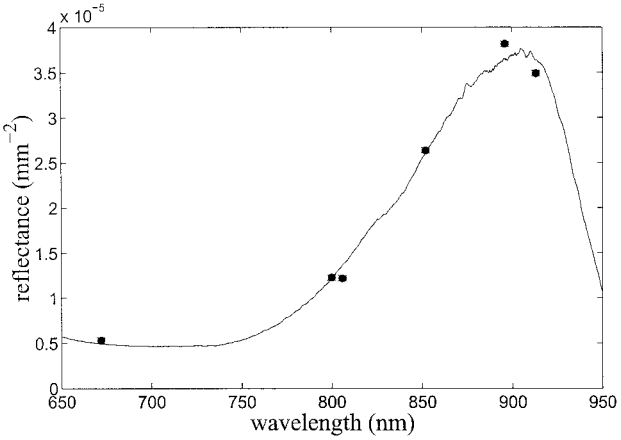

Fig. 2. SS reflectance spectrum acquired from a dye–Intralipid phantom, scaled to fit the discrete reflectance values (filled circles) predicted by Eqs. (1) and (2) with FD-derived values of μ_s' and μ_a. This scaling causes the entire spectrum to be converted into absolute reflectance units; see text for a discussion. The error in FD reflectance is estimated to be $\pm 3 \times 10^{-7}/\mathrm{mm}^{-2}$; in SS reflectance, $\pm 1 \times 10^{-7}/\mathrm{mm}^{-2}$.

tially the same scale factor. The entire SS spectrum is thus converted into absolute reflectance units. Similar results were observed for the three breast samples, as shown in Fig. 3. From top to bottom, sample 1 is the inner breast region of the 37-year-old volunteer and samples 2 and 3 are from the areolar border and the inner breast, respectively, of the 21-year-old volunteer.

Figure 4 shows the least-squares power-law fit to the μ_s' values measured by the FD on the phantom. As expected, the wavelength dependence is fairly smooth and is easily described by the fit. Corresponding fits for the three breast samples appear in Fig. 5. Note that the values change by only a factor

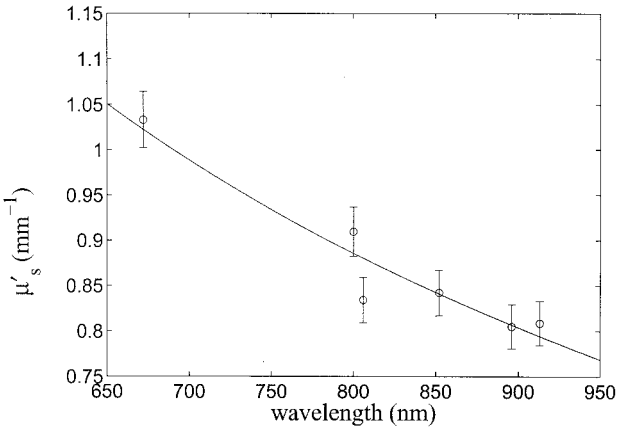

Fig. 4. Determination of the broadband μ_s' spectrum for the dye–Intralipid phantom. Open circles, discrete μ_s' values measured by the FD technique; solid curve, best power-law fit to Eq. (4). Fitting parameters are $A = 2200$ and $B = -0.82$. Error bars on μ_s' are 3%.[7]

of 2 over the entire range, so the wavelength dependence is weak in addition to being predictable.

Figure 6 summarizes the absorption values calculated for the dye–Intralipid phantom. The thicker curve shows the μ_a values that we found make Eq. (1) reproduce the measured reflectance data as closely as possible, using the fzero algorithm as described above. The thinner curve represents a linear least-squares fit to the thicker curve based on reference spectra of pure water (from Kou *et al.*[26]) and pure dye (measured by a spectrophotometer as described above). As the figure shows, the two-component fit accurately models the measured spectrum across the entire spectral range. The least-squares fitting coefficient for the dye spectrum is 1.00. Also shown are the values of μ_a derived by FD analysis alone, demonstrating an agreement between the FD and

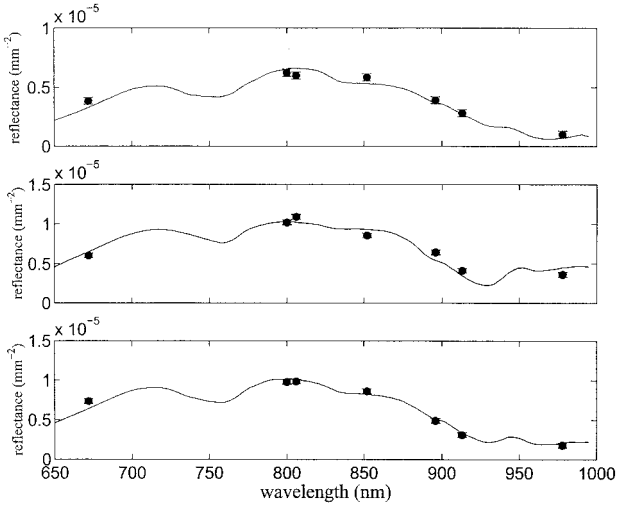

Fig. 3. SS reflectance spectra acquired from three locations in breast tissue of female volunteers. The spectra have been scaled to fit reflectance values (filled circles) calculated from FD data in the same manner as for Fig. 2. Errors are the same as for Fig. 2.

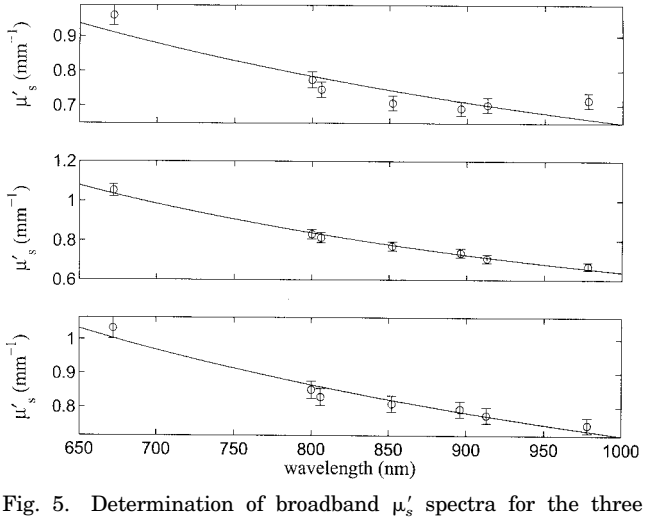

Fig. 5. Determination of broadband μ_s' spectra for the three breast samples. Circles, the discrete μ_s' values measured by the FD technique; solid curves, best power-law fits to Eq. (4). Fitting parameters (A, B) from top to bottom are (240, −0.86), (2700, −12), and (250, −0.85). Error bars on μ_s' are 3%.[7]

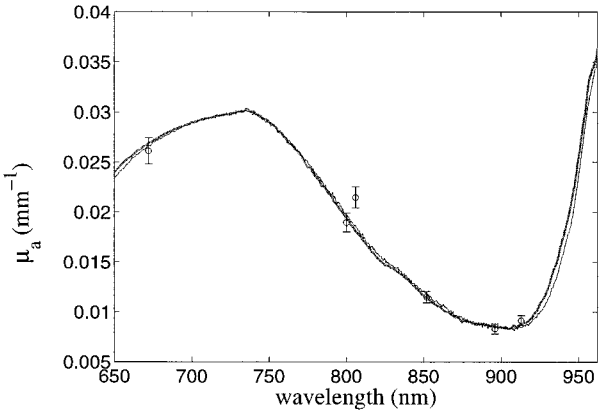

Fig. 6. Comparison of μ_a values generated by FD (open circles) and by SSFD (thicker curve) for the dye–Intralipid phantom. Also shown is the best fit (thinner curve) to the SSFD data by use of the spectra of naphthol (measured with a spectrophotometer) and of water (from Kou *et al.*[26]). Open circles, discrete μ_a values from FD alone. Error bars, ± 0.0005 mm^{-1} or 5%, whichever is larger.

SSFD methods at these wavelengths, as would be expected because the FD data have been used to calibrate the SS data.

Corresponding plots that show absorption spectra of the three breast samples appear in Figs. 7–9. As before, the thicker curve is the experimental data, the thinner curve is a full-spectrum fit, and the circles are FD values. In these cases, however, the fit is built from published spectra (see Fig. 10) of oxyhemoglobin, deoxyhemoglobin,[27] water,[26] and fat,[28] which are commonly regarded as the four major absorbers in breast tissue in the 650–1000-nm range. Coefficients from the fit thus provide estimates of these

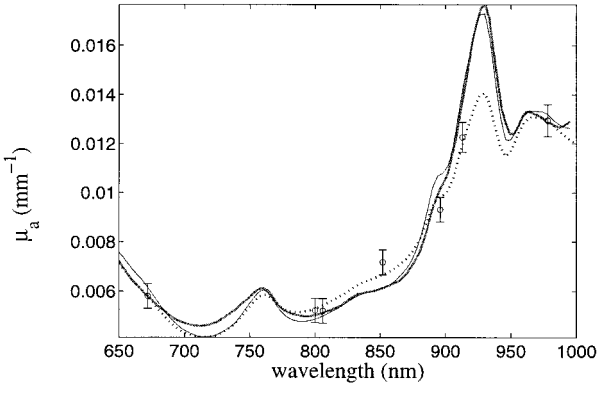

Fig. 7. μ_a predictions for the first breast measurement (inner breast; 37-year-old volunteer). Thicker curve, the SSFD data; thinner curve, least-squares fit for a superposition of Hb, HbO_2, water, and fat spectra; filled circles, the FD values (error bars, ± 0.0005 mm^{-1} or 5%, whichever is larger); dotted curve the least-squares fit when only the FD values are weighted. Physiological parameters from the SSFD spectral fit: total hemoglobin concentration, 22 μM; oxygen saturation, 73%; water, 15 g/cm^3; fat, 0.75 g/cm^3. See Table 1 for more details. Note that the fat peak between 900 and 950 nm is significantly underfitted by the FD calculation.

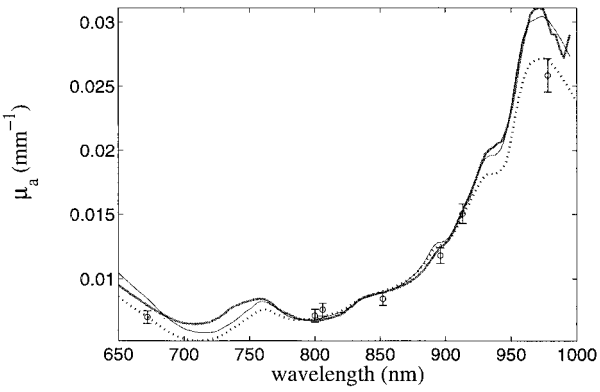

Fig. 8. μ_a predictions for the second breast measurement (areolar border; 21-year-old volunteer). Curves and circles have the same assignments as for Fig. 7. Physiological parameters: total hemoglobin concentration, 30 μM; oxygen saturation, 70%; water, 0.51 g/cm^3; fat, 0.42 g/cm^3. See Table 1 for more details.

components' concentrations. The estimates are useful for comparing one sample with another; no independent attempt to validate concentrations has been made (however, the concentrations are approximately correct in magnitude and, as we note in Section 6 below, the values are consistent with others from the recent literature[3,15]). For comparison purposes, the dotted curves in Figs. 7–9 show the spectral fit obtained when only the FD wavelengths are weighted, as in a customary FD-only experiment. The two spectral reconstructions are clearly different, and these different reconstructions lead to different concentration estimates. All the concentration predictions, both SSFD and FD, are listed in Table 1, along with the percent deviation of the FD value from the SSFD value. The hemoglobin results are reported in terms of total hemoglobin (oxyhemoglobin plus deoxyhemoglobin) and oxygen saturation (oxyhemoglobin divided by the total).

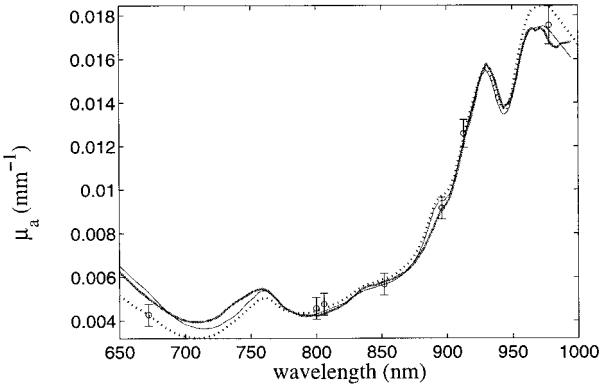

Fig. 9. μ_a predictions for the third breast measurement (inner breast; 21-year-old volunteer). Curves and circles have the same assignments as for Fig. 7. Physiological parameters: total hemoglobin concentration, 19 μM; oxygen saturation, 72%; water, 28 g/cm^3; fat, 0.56 g/cm^3. See Table 1 for more details.

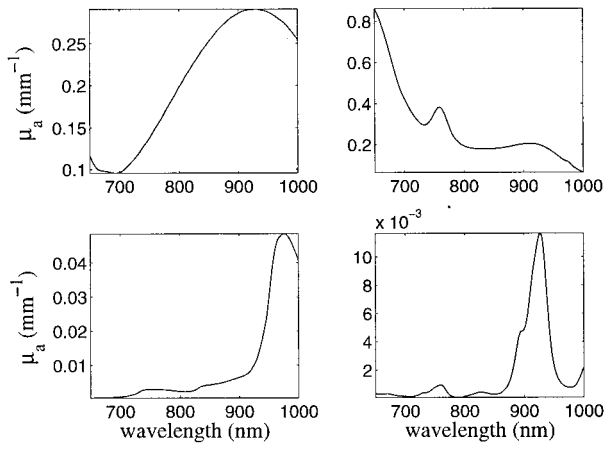

Fig. 10. Absorption spectra of major absorbers in breast tissue. Upper left, oxyhemoglobin, 1 μM; upper right, deoxyhemoglobin, 1 μM; lower left, water, 1 g/cm^3; lower right, fat (soybean oil), 0.9 g/cm^3. The hemoglobin spectra are from Wray *et al.*,[27] the water is from Kou *et al.*,[26] and the fat is from the doctoral dissertation of Eker.[28]

6. Discussion

To extract μ_a from a single SS reflectance spectrum, one has to convert the data into absolute units (i.e., the instrumental factor C_o must be removed) and determine μ_s' values at all wavelengths. We have demonstrated that FD measurements at a few wavelengths can accomplish these goals across the entire 650–1000-nm spectrum. This somewhat surprising result arises because $\mu_s'(\lambda)$ follows a power law, whereas C_o has no wavelength dependence at all. Two innovations that combine FD and SS methods are thus available. First, when the SS reflectance is scaled to match FD predictions of absolute reflectance, the entire reflectance spectrum is automatically calibrated. Second, fitting the FD μ_s' values to a wavelength-dependent function yields the extra information that one needs to extract μ_a from diffusion theory [Eqs. (1) and (2)]. We note that the FD-derived μ_a and μ_s' values could just as readily be supplied by time-domain measurements at a single source–detector separation.

The interpolation of the reduced scattering spectra by use of a fit is an important component of this technique. The lower two parts of Fig. 5 show excellent agreement with the power law. The top part of the figure shows reasonably good agreement, but small discrepancies (of the order of 5–8%) can nevertheless be observed. This behavior is likely not to be an actual divergence from the power law but is probably due to a coupling effect between the scattering and absorption quantification in the FD fit. Such coupling appears when the diffusion model's assumptions are not sufficiently fulfilled. The tissue heterogeneity, i.e., the layered superficial structure and the mix of deeper fat globules and fibrous tissue, could be a possible source of deviation from the model. Interestingly, the highest fat concentration was measured for this breast location (see Table 1). As described recently by Doornbos *et al.*,[15] using a power-law fit to calculate the μ_s' spectrum can in fact provide an advantage in computing μ_a. Indeed, by smoothing the spectrum, the power-law fit reduces the spurious coupling between scattering and absorption caused by inaccurate modeling.

Compared with discrete-wavelength FD measurements, access to a continuous absorption spectrum offers two important advantages: better chromophore identification and improved concentration quantification. The ability of the method to recover the continuous shape of the true absorption spectrum is evidenced by the phantom measurement. Figure 6 shows that the experimental spectrum is accurately fitted by use of known spectra of dye and water. The fitting coefficient of 1.00 for the dye additionally demonstrates the accurate recovery of chromophore concentrations.

The breast spectra (Figs. 7–9) further illustrate the usefulness of the SSFD technique for clinical investigations. As expected, the fit that uses oxyhemoglobin, deoxyhemoglobin, fat, and water accounts for most of the absorption in the 650–

Table 1. Results of Physiological Predictions for Breast Samples 1–3[a]

Breast Sample Number	Component	SSFD Method	FD Method Only	Percent Difference
1	Total Hb (μM)	22	25	13
	O_2 saturation (%)	73	78	7
	Water (g/cm^3)	0.15	0.14	−7
	Fat (g/cm^3)	0.75	0.44	−41
2	Total Hb (μM)	30	30	0
	O_2 saturation (%)	70	79	13
	Water (g/cm^3)	0.51	0.40	−22
	Fat (g/cm^3)	0.42	0.39	−7
3	Total Hb (μM)	19	19	0
	O_2 saturation (%)	72	81	13
	Water (g/cm^3)	0.28	0.27	−4
	Fat (g/cm^3)	0.56	0.54	−4

[a]Column 5 gives the percent difference between the FD and the SSFD values, defined as 100 × (FD − SSFD)/SSFD.

1000-nm range in breast tissue. The quality of the fit is especially striking for wavelengths longer than 800 nm. In particular, the fat spectrum used in the fit seems accurate, matching the main peak at 928 nm and the shoulder at 895 nm. These results are surprisingly good considering that the pure-fat spectrum was measured in soybean oil.[28] These measurements stress the important contribution of fat to tissue absorption, as this chromophore sometimes was neglected in previous research.[6,15] The water peak at 976 nm is also well reproduced in the measurements. We observe that the highest water content was measured for the areolar border sample (sample 2). Interestingly, we note that for both dye and breast tissue, data fits to the water spectrum of Kou *et al*. were superior to those of Hale and Querry,[29] particularly in the 920–960-nm regime where the water absorption spectrum increases sharply.

In the 650–800-nm region, the major features of tissue absorption are clearly due to oxyhemoglobin and deoxyhemoglobin. The deoxyhemoglobin peak at 760 nm is distinctly visible in the experimental data. Nevertheless, we observe small but consistent spectral differences, of the order of 0.001 mm^{-1}, between fit and measurement in this regime (see Figs. 7–9). These discrepancies, revealed in the full SSFD spectrum, are not evident when the FD data alone are fitted. Two reasons for the imperfect fits can be suggested. First, the oxyhemoglobin and deoxyhemoglobin absorption spectra that we used could be slightly incorrect. Indeed, small variations are found among various published spectra, and changes could be also expected between *in vitro* and *in vivo* values. Second, other, background, chromophores should probably be taken into account. For example, the tails of several protein absorption bands that were not included in the modeling might contribute to absorption in this wavelength region. A more extensive spectral library is therefore desirable for future studies. Alternatively, one could model the background empirically, either with predetermined mathematical functions of wavelength (see, e.g., Hull *et al*.[14]) or with a principal-component analysis of several background residuals once many samples have been studied.[30]

For the sake of comparison, we used the same least-squares fitting algorithm to calculate the spectral fits and concentrations twice, once with the full spectrum and once with only the FD wavelengths, even though the second procedure does not fully exploit the potential of the SSFD method. Interesting differences are found between the FD and SSFD calculations. Figure 7 and Table 1 show that FD significantly underestimates the fat concentration in the first breast sample: 0.75 g/cm^3 with the SSFD as opposed to 0.44 g/cm^3 with the FD. The reason for this discrepancy lies in the fact that no laser wavelength is close enough to the fat peak (at present, commercial laser diodes at this particular wavelength are uncommon). Thus, with no weighting in this region, the FD fit tolerates large fitting errors near the absorption maximum of fat (as illustrated in Fig. 7), leading to large errors in the fat concentration. Such a discrepancy is naturally enhanced for this sample, for which the fat concentration is highest. This example illustrates the shortcomings of using a limited number of sources (i.e., wavelengths), especially when a significant chromophore lies in an undersampled spectral region. A similar error is seen in the fitting of the areolar breast location (Fig. 8); this time it is the water peak that is poorly addressed by the FD analysis.

The total hemoglobin determination is more consistent between the FD and SSFD calculations, owing to the smoother spectral features of these chromophores and better diode coverage of the 650–850-nm regime. However, the oxygenation determination by FD is systematically higher. As discussed above, consistent small differences occur between the fit and the experiments in the 650–800-nm region because of some incompleteness in our library of fitting line shapes. Fitting the curve with a limited number of wavelengths naturally exacerbates the incompleteness and produces a bias in the results.

As mentioned above, Cubeddu *et al*.,[3] working in the time domain, obtained similar optical properties and physiological parameters for premenopausal breast. Conceptually, the two experiments exploit the same optical phenomena and are essentially complementary techniques in different domains. A technical advantage of the SSFD measurement is the use of a white-light source rather than a tunable laser. Thus the SS measurement covers all wavelengths simultaneously, whereas the laser(s) must be tuned separately to each wavelength.[3] Additionally, the heart of the SSFD system (a few laser diodes, a frequency generator, an avalanche photodiode, a network analyzer or lock-in amplifier, and a SS reflectance system) is inexpensive and easy to maintain compared with a tunable laser system and a single-photon-counting detection apparatus.

As was already stated, the method presented here has the advantage of being compatible with a single, large source–detector separation ($\gg$10 transport mean free paths). In contrast to spatially resolved methods, it is well suited for interrogating deep structures in relatively heterogeneous samples. As numerous authors have shown,[15,31,32] the layered structure of tissue affects reflectance differently at different source–detector separations, raising doubts about the applicability of spatially resolved techniques that assume sample homogeneity over a large range. Whereas variations in the FD modulation frequency ω do change the optically explored tissue volume, these effects are modest in comparison with changes in ρ, particularly at high absorption.[21] Consequently, the assumption of homogeneity is less extreme for the single-distance measurements proposed here: Its essence is that all measurements at one wavelength explore a more consistent volume; this does not

mean that different wavelengths will explore the same volume. Indeed, less-absorbed wavelengths will explore larger regions than wavelengths that attenuate more rapidly.

7. Conclusion

A combination of SS and FD reflectance measurements has been described for absorption spectroscopy of turbid media; beneficial aspects of both techniques have been described. As with SS, the wavelength coverage is continuous, detecting absorption features that may not be discernable in the discrete wavelengths chosen for FD. The prediction of constituent concentrations, for instance, in breast tissue, is substantially improved when full-spectrum absorption data rather than a handful of wavelengths are used. As with FD, however, only a single source–detector separation is required, making the technique more amenable to reporting volume-averaged values for heterogeneous samples. In addition, the source–detector separation can be large, allowing for centimeter-scale mean probing depths that cannot be achieved with spatially resolved SS techniques. This advantage for deeply probing studies is significant for many clinical purposes. An application to breast analysis has been demonstrated, with quantitative *in vivo* spectra of human breast obtained rapidly ($<$1 min). The total hemoglobin content, oxygen saturation, and water and fat content of the breast samples have been calculated from the spectra, and failures of FD-only fitting have been highlighted. The technique is relatively inexpensive and could prove valuable for improving accuracy in the development of quantitative photon migration for clinical instruments.

This study was supported by the National Institutes of Health under grants GM50958 and RR01192 (Laser Microbeam and Medical Program), the U.S. Department of Energy (grant DE-FG03-91ER61227), and the U.S. Office of Naval Research (grant N00014-91-C-0134). The authors gratefully acknowledge postdoctoral fellowships: A. J. Berger from the George E. Hewitt Foundation for Medical Research; F. Bevilacqua from the Swiss National Science Foundation; and A. E. Cerussi from the U.S. Army (grant DAMD17-98-1-8186.) We used the facilities and support of the Avon Breast Center of the Chao Family Comprehensive Cancer Center at the University of California, Irvine, to complete clinical portions of this study.

References

1. M. S. Patterson, B. Chance, and B. C. Wilson, "Time resolved reflectance and transmittance for the noninvasive measurement of tissue optical properties," Appl. Opt. **28,** 2331–2336 (1989).
2. A. Kienle and M. S. Patterson, "Improved solutions of the steady-state and the time-resolved diffusion equations for reflectance from a semi-infinite medium," J. Opt. Soc. Am. **14,** 246–254 (1997).
3. R. Cubeddu, A. Pifferi, P. Taroni, A. Torricelli, and G. Valentini, "Noninvasive absorption and scattering spectroscopy of bulk diffusive media: an application to the optical characterization of human breast," Appl. Phys. Lett. **74,** 874–876 (1999).
4. B. W. Pogue and M. S. Patterson, "Frequency-domain optical absorption spectroscopy of finite tissue volumes using diffusion theory," Phys. Med. Biol. **39,** 1157–1180 (1994).
5. S. Fantini, M. A. Franceschini-Fantini, J. S. Maier, S. A. Walker, B. Barbieri, and E. Gratton, "Frequency-domain multichannel optical detector for noninvasive tissue spectroscopy and oximetry," Opt. Eng. **34,** 32–42 (1995).
6. J. B. Fishkin, O. Coquoz, E. R. Anderson, M. Brenner, and B. J. Tromberg, "Frequency-domain photon migration measurements of normal and malignant tissue optical properties in a human subject," Appl. Opt. **36,** 10–20 (1997).
7. T. H. Pham, O. Coquoz, J. B. Fishkin, E. Anderson, and B. J. Tromberg, "Broad bandwidth frequency domain instrument for quantitative tissue optical spectroscopy," Rev. Sci. Instrum. **71,** 2500–2513 (2000).
8. L. Reynolds, C. Johnson, and A. Ishimaru, "Diffuse reflectance from a finite blood medium: applications to the modeling of fiber optic catheters," Appl. Opt. **15,** 2059–2067 (1976).
9. T. J. Farrell, M. S. Patterson, and B. C. Wilson, "A diffusion theory model of spatially resolved, steady-state diffuse reflectance for the noninvasive determination of tissue optical properties *in vivo*," Med. Phys. **19,** 879–888 (1992).
10. A. Kienle, L. Lilge, M. S. Patterson, R. Hibst, R. Steiner, and B. C. Wilson, "Spatially resolved absolute diffuse reflectance measurements for noninvasive determination of the optical scattering and absorption coefficients of biological tissue," Appl. Opt. **35,** 2304–2314 (1996).
11. R. Bays, G. Wagnières, D. Robert, D. Braichotte, J.-F. Savary, P. Monnier, and H. van den Bergh, "Clinical determination of tissue optical properties by endoscopic spatially resolved reflectometry," Appl. Opt. **35,** 1756–1766 (1996).
12. R. A. Weersink, J. Hayward, K. Diamond, and M. Patterson, "Accuracy of noninvasive *in vivo* measurements of photosensitizer uptake based on a diffusion model of reflectance spectroscopy," Photochem. Photobiol. **66,** 326–335 (1997).
13. F. Bevilacqua, D. Piguet, P. Marquet, J. Gross, B. Tromberg, and C. Depeursinge, "*In vivo* local determination of tissue optical properties: applications to human brain," Appl. Opt. **38,** 4939–4950 (1999).
14. E. L. Hull, M. G. Nichols, and T. H. Foster, "Quantitative broadband near-infrared spectroscopy of tissue-stimulating phantoms containing erythrocytes," Phys. Med. Biol. **43,** 3381–3404 (1998).
15. R. M. P. Doornbos, R. Lang, M. C. Aalders, F. W. Cross, and H. J. C. M. Sterenborg, "The determination of *in vivo* human tissue optical properties and absolute chromophore concentrations using spatially resolved steady-state diffuse reflectance spectroscopy," Phys. Med. Biol. **44,** 967–981 (1999).
16. B. J. Tromberg, O. Coquoz, J. B. Fishkin, T. Pham, E. R. Anderson, J. Butler, M. Cahn, J. D. Gross, V. Venugopalan, and D. Pham, "Non-invasive measurements of breast tissue optical properties using frequency-domain photon migration," Phil. Trans. R. Soc. London **352,** 661–668 (1997).
17. A. Ishimaru, *Wave Propagation and Scattering in Random Media* (Academic, Orlando, Fla., 1978).
18. J. B. Fishkin and E. Gratton, "Propagation of photon-density waves in strongly scattering media containing an absorbing semi-infinite plane bounded by a straight edge," J. Opt. Soc. Am. **10,** 127–140 (1993).
19. B. J. Tromberg, L. O. Svaasand, T.-T. Tsay, and R. C. Haskell, "Properties of photon density waves in multiple-scattering media," Appl. Opt. **32,** 607–616 (1993).
20. S. Fantini, M. A. Franceschini, J. B. Fishkin, B. Barbieri, and E. Gratton, "Quantitative determination of the absorption

spectra of chromophores in strongly scattering media: a light-emitting-diode based technique," Appl. Opt. **33,** 5204–5213 (1994).
21. R. C. Haskell, L. O. Svaasand, T.-T. Tsay, T.-C. Feng, M. S. McAdams, and B. J. Tromberg, "Boundary conditions for the diffusion equation in radiative transfer," J. Opt. Soc. Am. **11,** 2727–2741 (1994).
22. W. H. Press, S. A. Teukolsky, W. T. Vetterling, and B. P. Flannery, in *Numerical Recipes in C: The Art of Scientific Computing*, 2nd ed. (Cambridge U. Press, Cambridge, 1993), Chap. 15, pp. 683–688.
23. R. Graaff, J. G. Aarnoose, J. R. Zijp, P. M. A. Sloot, F. F. M. de Mul, J. Greve, and M. H. Koelink, "Reduced light-scattering properties for mixtures of spherical particles: a simple approximation derived from Mie calculations," Appl. Opt. **31,** 1370–1376 (1992).
24. J. R. Mourant, T. Fuselier, J. Boyer, T. Johnson, and I. J. Bigio, "Predictions and measurements of scattering and absorption over broad wavelength ranges in tissue phantoms," Appl. Opt. **36,** 949–957 (1997).
25. J. M. Schmitt and G. Kumar, "Optical scattering properties of soft tissue: a discrete particle model," Appl. Opt. **37,** 2788–2797 (1998).
26. L. H. Kou, D. Labrie, and P. Chylek, "Refractive indices of water and ice in the 0.65- to 2.5-μm spectral range," Appl. Opt. **32,** 3531–3540 (1993).
27. S. Wray, M. Cope, D. T. Delpy, J. S. Wyatt, and E. O. R. Reynolds, "Characterization of the near-infrared absorption spectra of cytochrome-AA3 and hemoglobin for the noninvasive monitoring of cerebral oxygenation," Biochim. Biophys. Acta **933,** 184–192 (1988).
28. C. Eker, *Optical Characterization of Tissue for Medical Diagnostics*, Ph.D. dissertation (Lund University, Lund, Sweden, 1999).
29. G. M. Hale and M. R. Querry, "Optical constants of water in the 200-nm to 200-μm wavelength region," Appl. Opt. **12,** 555–563 (1973).
30. A. J. Berger, T.-W. Koo, I. Itzkan, and M. S. Feld, "An enhanced algorithm for linear multivariate calibration," Anal. Chem. **70,** 623–628 (1998).
31. G. Alexandrakis, T. J. Farrell, and M. S. Patterson, "Accuracy of the diffusion approximation in determining the optical properties of a two-layer turbid medium," Appl. Opt. **37,** 7401–7409 (1998).
32. M. A. Franceschini, S. Fantini, L. A. Paunescu, J. S. Maier, and E. Gratton, "Influence of a superficial layer in the quantitative spectroscopic study of strongly scattering media," Appl. Opt. **37,** 7447–7458 (1998).